Effect of proton irradiation on the normal-state low-energy excitations of $Ba(Fe_{1-x}Rh_x)_2As_2$ superconductors

M. Moroni,[1,*] L. Gozzelino,[2,3] G. Ghigo,[2,3] M. A. Tanatar,[4] R. Prozorov,[4] P. C. Canfield,[4] and P. Carretta[1]

[1]*Department of Physics, University of Pavia-CNISM, I-27100 Pavia, Italy*

[2]*Istituto Nazionale di Fisica Nucleare, Sez. Torino, Torino 10125, Italy*

[3]*Politecnico di Torino, Dept. of Applied Science and Technology, 10129 Torino, Italy*

[4]*Ames Laboratory USDOE and Department of Physics and Astronomy, Iowa State University, Ames, Iowa 50011, USA*

(Received 17 May 2017; revised manuscript received 30 August 2017; published 19 September 2017)

We present a ^{75}As nuclear magnetic resonance (NMR) and resistivity study of the effect of 5.5 MeV proton irradiation on the optimal electron doped ($x = 0.068$) and overdoped ($x = 0.107$) $Ba(Fe_{1-x}Rh_x)_2As_2$ iron based superconductors. While the proton induced defects only mildly suppress the critical temperature and increase residual resistivity in both compositions, sizable broadening of the NMR spectra was observed in all the irradiated samples at low temperature. The effect is significantly stronger in the optimally doped sample where the Curie Weiss temperature dependence of the line width suggests the onset of ferromagnetic correlations coexisting with superconductivity at the nanoscale. $1/T_2$ measurements revealed that the energy barrier characterizing the low energy spin fluctuations of these compounds is enhanced upon proton irradiation, suggesting that the defects are likely slowing down the fluctuations between $(0,\pi)$ and $(\pi,0)$ nematic ground states.

DOI: 10.1103/PhysRevB.96.094523

I. INTRODUCTION

Chemical substitution is the most common approach used to introduce impurities in strongly correlated electron systems in order to probe their local response function. However, this method often gives rise to structural distortions, unwanted inhomogeneity, and charge doping. Accordingly, in order to study the effect of the bare impurities, the right dopant must be carefully chosen and the options are often very limited. Thus irradiation with energetic particles, electrons and ions, may represent a powerful alternative to chemical substitutions. Radiation induced defects have been extensively employed in high temperature superconductors to investigate the pair breaking effect of nonmagnetic scattering centers and to study the pinning of the Abrikosov vortices. In particular, heavy ions irradiation (e.g., with Au and Pb) induces strongly anisotropic columnar defects, which are effective in pinning the flux vortices [1,2]. Conversely, low mass ions, such as protons, α particles, or electrons, give rise to uniformly distributed pointlike defects whose density can be precisely controlled. In the cuprates the decrease of the superconducting transition temperature T_c with the radiation fluence ϕ was found to strongly depend on the ion type, on its energy, and on the total dose [3]. Remarkably, in $YBa_2Cu_3O_{7-\delta}$ and $Tl_2Ba_2CuO_{6+x}$, it was found [4] that the defects introduced by electron irradiation play a role analogous to nonmagnetic Zn impurities, and the magnitude of $dT_c/d\phi$ is consistent with the theoretical prediction for a d-wave superconductor [5].

In the iron based superconductors (IBS) several irradiation studies have been conducted with heavy [2,6–12] ions, light ions [9,11,13–15], and electrons [16–21]. In these compounds T_c suppression by radiation damage is rather weak for optimally doped compositions but becomes stronger in underdoped and overdoped compositions. Simultaneous studies of T_c suppression and London penetration depth as a function of doping in $Ba_{1-x}K_xFe_2As_2$ [17,20] conclude that both quantities can be reasonably fit to the $s^{\pm}$ model [22,23] which is the leading candidate for describing the pairing state in most of the IBS [24–26]. Interestingly, these results are consistent with the reduced T_c suppression induced by nonmagnetic Zn doping in $Ba(Fe_{1-x}Co_x)_2As_2$ and $LaFeAsO_{1-x}F_x$ [27–30]. This weak effect of diamagnetic impurities in IBS is not necessarily an indication of a different gap symmetry. In fact one should notice that the defects weaken also the spin density wave (SDW) phase competing with superconductivity (SC) in the underdoped part of the phase diagram [24,31,32]. Hence, $dT_c/d\phi$ strongly depends on the system parameters in the underdoped regime, both for proton irradiation and nonmagnetic Zn doping [13,14,27–30].

The studies cited above focus mainly on the superconducting state and no reports can be found in the literature on a systematic investigation of the effects of irradiation on the normal state properties of IBS, in particular on the spin and nematic correlations [33]. In 122 iron based superconductors very slow spin fluctuations have been detected above T_c with nuclear magnetic resonance (NMR) [34–36] and have been ascribed to nematic fluctuations among $(0,\pi)$ and $(\pi,0)$ correlated regions [37]. Recently ^{75}As $1/T_2$ NMR measurements in electron doped $Ba(Fe_{1-x}Rh_x)_2As_2$ revealed [38,39] that these fluctuation are not only present in the underdoped part of the phase diagram but extend up to at least 11% Rh doping, well into the overdoped regime.

In this paper we show that proton induced defects significantly affect the slow spin fluctuations revealed by ^{75}As$1/T_2$ in $Ba(Fe_{1-x}Rh_x)_2As_2$, suggesting that the fluctuations developing between $(0,\pi)$ and $(\pi,0)$ phases are affected by the disorder. Moreover, we observe a broadening of the ^{75}As NMR spectra induced by proton irradiation and for the optimally doped 0.068 Rh sample the defects induce ferromagnetically correlated regions around the impurities, coexisting with superconductivity.

*matteo.moroni01@universitadipavia.it

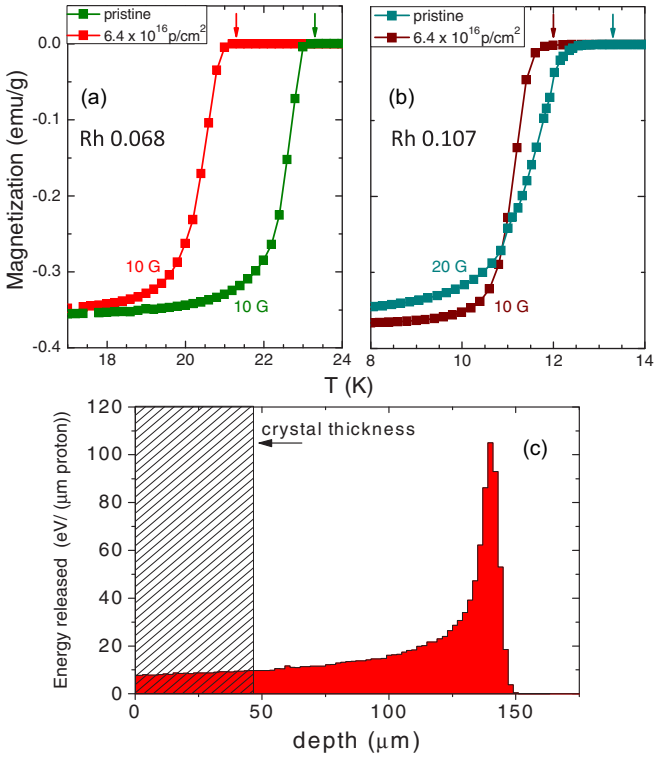

FIG. 1. (a), (b) Zero field cooling SQUID magnetization measurements for the $x = 0.068$ sample (a) and $x = 0.107$ sample (b) carried out before and after irradiation. The arrows indicate T_c as determined by the onset of diamagnetism. The magnetic field value used for the measurements is 10 G for the $x = 0.068$ sample and for the irradiated $x = 0.107$ sample, while it is 20 G for the pristine $x = 0.107$ sample. (c) Distribution of the proton energy loss in the superconducting crystals (less than 50 μm thick) as a function of depth. The thickness of the thickest irradiated sample is about 45 μm, as evidenced in the picture. Therefore, the energy release can be considered homogeneous throughout the crystals, as well as the distribution of defects.

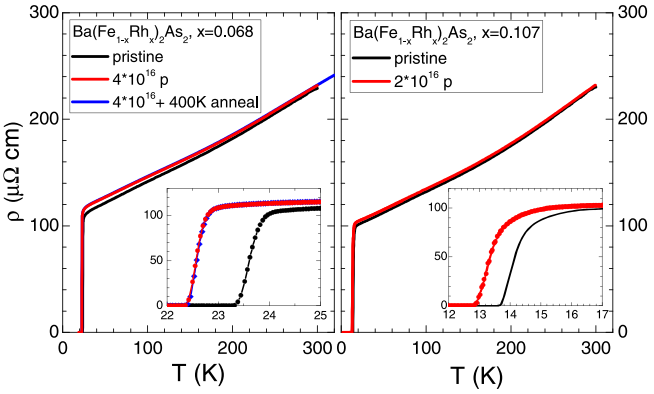

FIG. 2. Temperature-dependent electrical resistivity $\rho(T)$ of optimally doped $x = 0.068$ (left panel) and overdoped $x = 0.107$ (right panel) samples of $Ba(Fe_{1-x}Rh_x)_2As_2$. Insets zoom into superconducting transition range. Black lines show $\rho(T)$ for samples in the pristine state; red lines show the data for the same samples after proton irradiation. Blue line in the left panel shows $\rho(T)$ of the same sample after annealing at 400 K, revealing permanent character of proton irradiation damage, in contrast to damage by electron irradiation [17]. Note nonparallel shift of the $\rho(T)$ curves after irradiation, revealing Matthiessen rule violation.

II. EXPERIMENTAL METHODS AND RESULTS

The measurements presented in this work were performed on $Ba(Fe_{1-x}Rh_x)_2As_2$ single crystals with Rh content of $x = 0.068$ (optimally doped sample) and $x = 0.107$ (overdoped sample). The crystals were grown using the method described in Ref. [40]. The samples were then characterized by means of SQUID magnetometry (see Fig. 1) and resistivity measurements (see Figs. 2 and 3). Electrical resistivity measurements were carried out using the four-probe technique on cleaved samples with typical dimensions $2 \times 0.5 \times 0.05$ mm^3, with the long dimension corresponding to [100] crystallographic direction. Low resistance contacts to the samples were made by soldering 50 μm Ag wires using Sn [41–43]. Measurements were made on six samples of $x = 0.068$ and seven samples of $x = 0.107$. In both cases resistivity of the samples at room temperature $\rho(300\,\mathrm{K})$ was 230 ± 30 $\mu\Omega$ cm (see Fig. 2), consistent within error bars with the results for Co-doped compositions of similar x [44].

Selected crystals of each batch were then irradiated with 5.5 MeV protons at the CN Van de Graaff accelerator of INFN-LNL (Istituto Nazionale di Fisica Nucleare - Laboratori Nazionali di Legnaro, Italy). Contacts to the samples remained intact during irradiation, thus eliminating uncertainty of geometric factor determination and enabling quantitative comparison of resistivity measurements. To minimize the heating of the crystals under irradiation the proton flux was always limited to 10^{12} cm^{-2} s^{-1}.

The irradiation with 5.5 MeV protons produces random point defects and some defect nanoclusters, due to elastic scattering of protons against the target nuclei [13–15]. The thickness of the crystals was much smaller than the proton implantation depth, as calculated by the SRIM-2013 code [45]

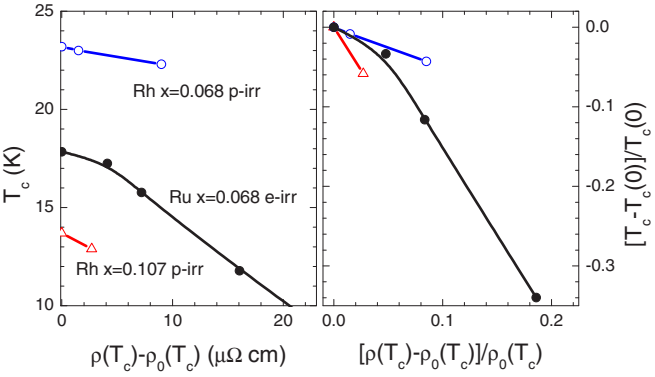

FIG. 3. (Left panel) The superconducting transition temperature T_c as a function of change in sample resistivity $\rho(T_c)$ for samples of $Ba(Fe_{1-x}Rh_x)_2As_2$ with optimal doping $x = 0.068$ (blue curve, open circles) and $x = 0.107$ (red curve, open up-triangles). For reference we show data for isoelectron substituted $Ba(Fe_{1-x}Ru_x)_2As_2$ at optimal doping $x = 0.24$, subject to low-temperature 2.5 MeV electron irradiation, Ref. [17]. Right panel shows the same data plotted as the change in T_c and resistivity $\rho(T_c)$ normalized by their values in pristine samples $T_c(0)$ and $\rho_0(T_c)$.

TABLE I. Summary of the average displacements per atom (dpa) and distance between defects as a function of the proton irradiation fluences.

ϕ (cm^{-2})	dpa	Interdefect distance (nm)
2×10^{16}	5.1×10^{-4}	3.5
3.2×10^{16}	8.2×10^{-4}	3
4×10^{16}	1×10^{-3}	2.8
6.4×10^{16}	1.6×10^{-3}	2.4

using the Kinchin-Pease approach, that is the recommended procedure for the evaluation of the displacement damage [46]. This ensured a homogeneous defect distribution in the superconductor, as evidenced by Fig. 1(c) where the energy lost by protons due to elastic scattering is plotted as a function of the implantation depth. In Table I the average displacement damage (dpa: displacements per atom) and the inferred average distance between proton-induced point defects are reported as a function of the irradiation fluence. This approach does not give a direct evaluation of Fe, Ba, and As atoms displaced in the irradiation process. However, since SRIM models the target as amorphous and selects the target atoms just taking into account their stoichiometric abundance, it is implicitly assumed that 20% of displacements involve Ba, 37.3% Fe, 40% As, and 2.7% Rh, which means that the defects mainly affect the superconducting layer. It has to be noted that the distance between defects should be assumed as a lower limit since the primary point defects (Frenkel pairs) could migrate to form small clusters and some defects could anneal out. After crossing the whole crystals thickness protons get implanted into the sample holder.

After irradiation the samples were again characterized with resistivity measurements to check the reduction of T_c and ^{75}As NMR measurements were then carried out. Figure 2 shows temperature dependent resistivity of the samples $x = 0.068$ (left panel) and $x = 0.107$ (right panel) before and after irradiation. Sample $x = 0.068$ was subject to a fluence up to 4×10^{16}cm^{-2}, which resulted in approximately 1 K decrease of T_c from 23.3 K to 22.3 K as determined by zero resistance criterion. Resistivity above the transition increased from 106 to 115 $\mu\Omega$ cm. To check the stability of irradiation damage, one sample of $x = 0.068$ was heated up to 400 K. This protocol is known to show significant T_c restoration and residual resistivity decrease in electron irradiated samples [17], none of which is observed for proton irradiation. Due to a two times smaller irradiation fluence, 2×10^{16} cm^{-2}, T_c suppression in samples of $x = 0.107$ is somewhat smaller, $\Delta T_c \approx 0.8$ K, from 13.7 to 12.9 K. Resistivity increase is also notably smaller, $\Delta\rho \approx 3\ \mu\Omega$ cm.

It should be noticed that, for both compositions, the resistivity increase after irradiation is not a rigid offset as one would expect from the Matthiessen rule. The shift becomes notably larger at low temperatures, in line with observations on hole-doped $Ba_{1-x}K_xFe_2As_2$ [19]. In Fig. 3 we plot the effect of irradiation on T_c as a function of the residual resistivity change with respect to pristine sample $\rho(T_c) - \rho_0(T_c)$. In the right panel we plot the same data normalized by the values in the pristine sample. For reference we plot the data for isoelectron substituted $Ba(Fe_{1-x}Ru_x)_2As_2$ at optimal doping $x = 0.24$, irradiated with 2.5 MeV electrons [17]. For low fluence values the rates of T_c variation are comparable in both cases, with some differences which can be ascribed to the variation of response due to the variation of doping level, rather than to the type of disorder. This is quite remarkable considering the very different annealing effect in the two cases and suggests that irradiations with protons and electrons of some MeV energy provide a similar kind of defect, even if only the former produces annealing-resistant damage.

T_c was also measured *in situ* during the NMR experiment by monitoring the detuning temperature of the NMR resonating circuit. The decrease of T_c after irradiation ($\phi = 3.2 \times 10^{16}$ cm^{-2}) was found to be small both for the $x = 0.068$ (from 23.3 K before irradiation to ~22 K afterwards) and for the $x = 0.107$ (from ~13.3 K to ~12.5 K). The samples were then irradiated again to increase the total fluence to $\phi = 6.4 \times 10^{16}$ cm^{-2}, and SQUID [see Figs. 1(a) and 1(b)] and NMR measurements were repeated. The expected displacement damage after these second irradiations and the corresponding average distance between proton-induced point defects are reported in Table I. The second irradiation lowered T_c to 21.3 K for $x = 0.068$ and to 12 K for $x = 0.107$. Hence, the T_c decrease rate is $dT_c/d\phi \simeq 0.3 \times 10^{-16}$ K cm^2 for the optimally doped sample and about 0.2×10^{-16} K cm^2 for the overdoped one.

The values of $dT_c/d\phi$ are lower than those observed in $Ba(Fe_{1-x}Co_x)_2As_2$ and $Ba_{1-x}K_xFe_2As_2$ irradiated with 3 MeV protons [13,14]. This effect was expected since the nonionizing energy loss, which drives the number of defects produced per incoming proton, decreases if the energy of the incoming proton is increased [3]. This means that, somewhat counterintuitively, the effectiveness of protons in damaging the lattice decreases by increasing their energy.

For each sample doping and dose value we measured the temperature dependence of the ^{75}As NMR linewidth, of the spin-lattice relaxation rate ($1/T_1$) and of the spin-spin relaxation rate ($1/T_2$). The magnetic field $\mathbf{H}_0 = 7$ T was applied along the crystallographic c axis unless otherwise specified.

The full width at half maximum ($\Delta\nu$ hereafter) of the ^{75}As central line ($m_I = \frac{1}{2} \rightarrow -\frac{1}{2}$) was derived from the fast Fourier transform of half of the echo signal after a standard Hahn spin-echo pulse sequence ($\pi/2 - \tau - \pi$, with a $\pi/2$ pulse length of $= 2.5\ \mu$s). The results for the optimally doped sample are shown in Fig. 4 and those for the overdoped crystal can be found in Fig. 5.

In the $x = 0.068$ sample the linewidth increases significantly upon cooling, following a Curie-Weiss law for all doses. Conversely, for $x = 0.107$, $\Delta\nu$ remains nearly flat down to T_c in the nonirradiated sample while it slowly increases, reaching a maximum around 20 K, in the irradiated one. These strikingly different $\Delta\nu$ behaviors will be discussed in the next section.

The ^{75}As spin-lattice relaxation rate was estimated by fitting the recovery of the longitudinal magnetization $M_z(t)$ after a saturation recovery pulse sequence ($\pi/2 - \tau - \pi/2 - \tau_{\text{echo}} - \pi$) with the standard recovery function for the central line of a spin 3/2 nucleus:

$$M_z(\tau) = M_0[1 - f\,(0.1 \cdot e^{-(\tau/T_1)} + 0.9 \cdot e^{-(6\tau/T_1)})]\,. \quad (1)$$

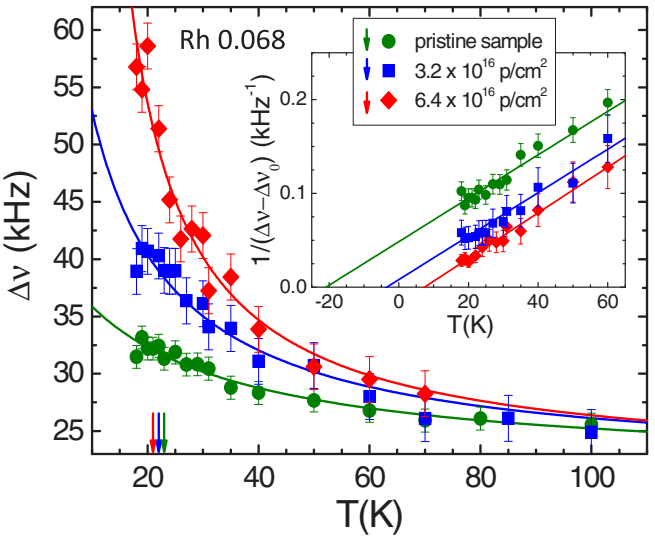

FIG. 4. Temperature dependence of the full width at half maximum $\Delta\nu$ for the ^{75}As central line in the $x = 0.068$ sample. The solid lines are fits to a Curie-Weiss law (see text). Inset: Inverse of the temperature dependent component of the line width. The intercepts of the linear fits with the x axis correspond to $-\theta$ (see text). The arrows indicate T_c for each radiation dose.

The results, displayed in Fig. 6, clearly show that $1/T_1$ is unaffected by the presence of proton induced defects. In particular, the spin-lattice relaxation follows a power law $1/T_1 \sim T^{\alpha}$, with $\alpha \simeq 0.6$ for the $x = 0.068$ sample and $\alpha \simeq 1$ for the $x = 0.107$ sample, namely close to the Korringa behavior expected for a weakly correlated metal.

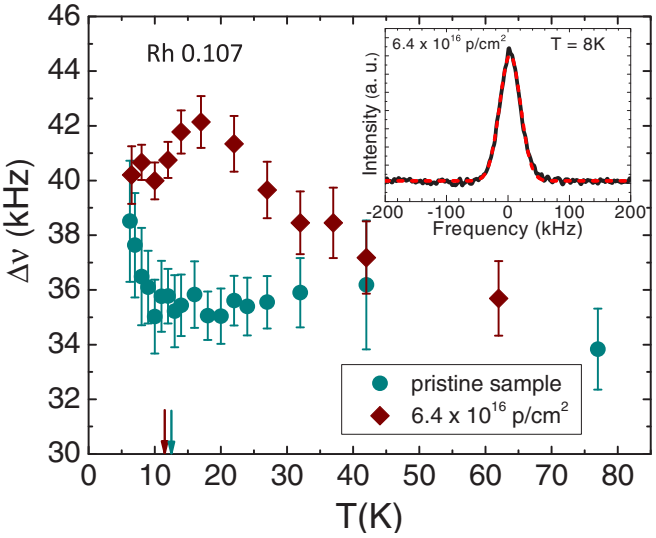

FIG. 5. Temperature dependence of the linewidth (FWHM) for the ^{75}As central line in the $x = 0.107$ sample. In the inset a low temperature ^{75}As NMR spectrum is shown; the dashed line is a fit to a gaussian function. The arrows indicate T_c for each radiation dose. The line width data for the $\phi = 3.2 \times 10^{16}$ cm^{-2} dose level are pretty similar to those for $\phi = 6.4 \times 10^{16}$cm^{-2} and have not been reported to improve the figure readability.

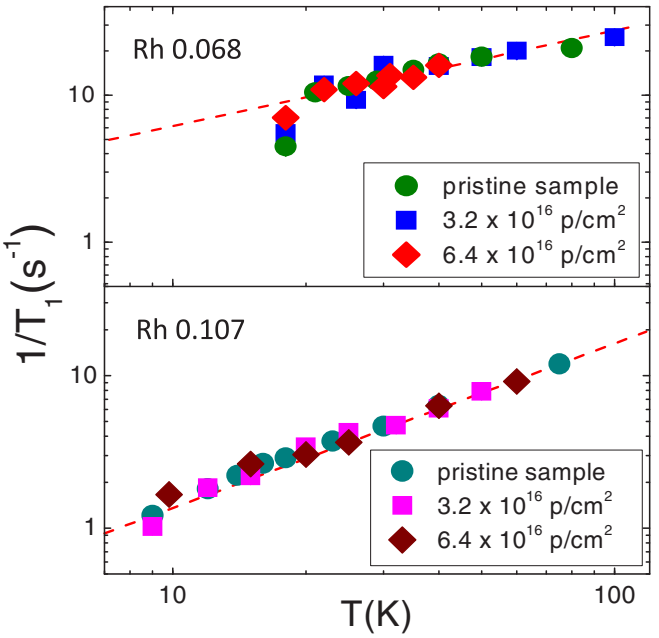

FIG. 6. Temperature dependence of the ^{75}As $1/T_1$ measured with H $\parallel$ c for the $x = 0.068$ (top) and $x = 0.107$ (bottom) samples. The red dashed lines are guides to the eye.

The spin echo decay rate $(1/T_2)$ was evaluated by recording the decay of the spin-echo amplitude $M_{\text{total}}(2\tau)$ after a spin echo pulse sequence. Since at high temperatures the values of T_1 and T_2 are in the same range (5–100 ms), the T_1 contribution to the spin echo decay is not negligible (Redfield term [47]). Within this framework the echo decay amplitude $M_{\text{total}}(2\tau)$ can be written as [48]:

$$M_{\text{total}}(2\tau) = M(2\tau)\exp\left(-\frac{2\tau}{T_{1R}}\right), \tag{2}$$

where $M(2\tau)$ is the T_1 independent echo decay amplitude while the exponential term takes into account the T_1 contribution. Walstedt and coworkers [48] found that, for the central line of a 3/2 spin nucleus, $1/T_{1R}$ is:

$$\frac{1}{T_{1R}} = \frac{3}{T_1^{\parallel}} + \frac{1}{T_1^{\perp}}\,, \tag{3}$$

where $T_1^{\parallel}$ and $T_1^{\perp}$ denote the spin lattice relaxation rate measured with the static magnetic field parallel and perpendicular to the crystallographic c axis, respectively. The raw echo amplitude was then divided by $\exp(-\frac{2\tau}{T_{1R}})$ in order to derive $M(2\tau)$. It was found that $M(2\tau)$ deviates from a single exponential decay (see Fig. 7) and could be fitted, over the whole temperature range, by a stretched exponential:

$$M(2\tau) = M_0\exp\left(-\left(\frac{2\tau}{T_2}\right)^{\beta}\right), \tag{4}$$

with β the stretching exponent.

The values of β are strongly temperature dependent (Fig. 7): at high temperature $\beta \simeq 2$, indicating a Gaussian decay of the spin echo, while it gradually decreases upon lowering the temperature, reaching $\beta \simeq 1$ (simple exponential) close to T_c, see Figs. 7(c)–7(d).

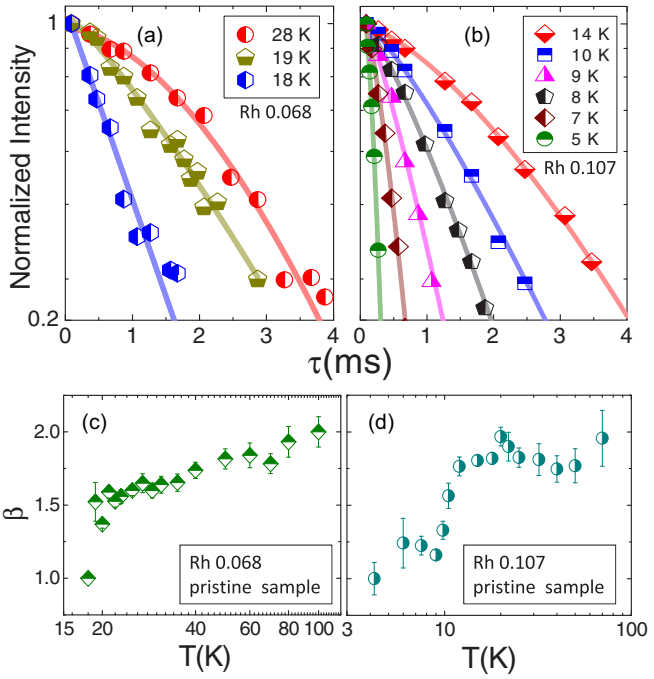

FIG. 7. Spin echo decay amplitude $M(2\tau)$ for the optimally doped $x = 0.068$ (a) and overdoped $x = 0.107$ (b) samples irradiated with a fluence of 6.4×10^{16} cm^{-2}, after dividing for Redfield contribution (see text). The solid lines are fits to a stretched exponential decay function (see text). The two lower panels [(c) and (d)] show the temperature evolution of the stretching exponent β resulting from the fit of the spin echo decay with Eq. (4) for the pristine samples. The results for the irradiated samples are nearly identical, well within the error bars of the β value of the pristine samples.

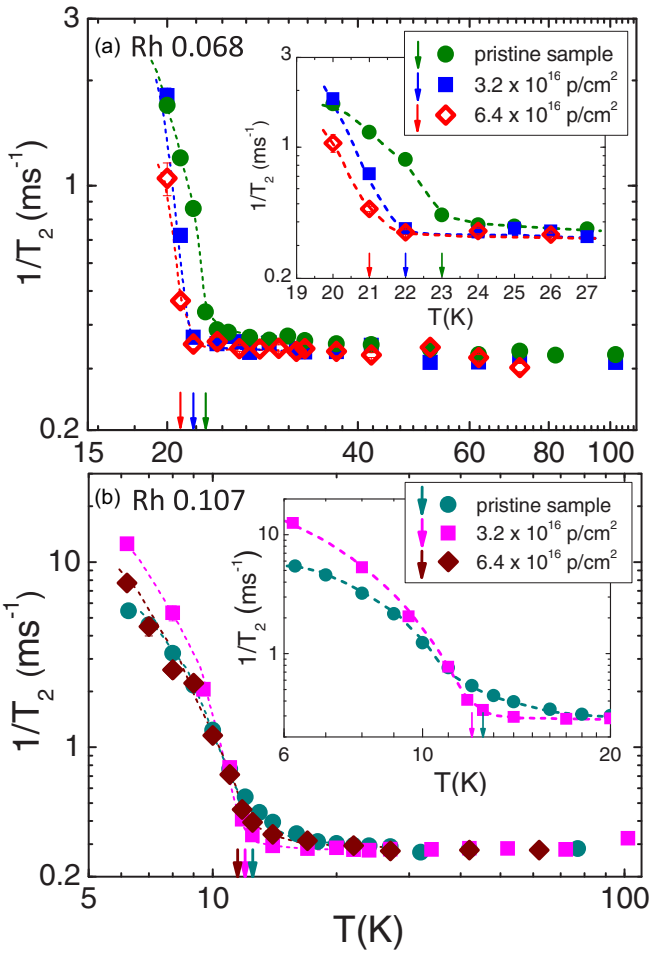

FIG. 8. Temperature dependence of the ^{75}As $1/T_2$ relaxation rate of the $x = 0.068$ (top) and $x = 0.107$ (bottom) samples for different values of fluence (see legend). In the insets the low temperature data are shown in greater detail. The arrows indicate T_c for each radiation dose and Rh doping level. The dashed lines are guides to the eye.

The decrease of beta above T_c indicates the onset of a low frequency dynamic as thoroughly explained in Ref. [36]. The temperature dependence of $1/T_2$ upon varying the dose and Rh doping is displayed in Fig. 8.

While at temperatures much higher than T_c the spin echo decay rate is flat for both compounds, a sharp rise in $1/T_2$ was observed just above T_c. This effect has already been reported in previous studies (see Refs. [38,39]) and is clearly decoupled from T_c. In fact, by increasing the static magnetic field [39] it is possible to shift the $1/T_2$ increase to much higher temperatures. As can be seen in insets of Fig. 8, the $1/T_2$ upturn becomes sharper in the proton irradiated samples.

If we define T^* as the temperature below which $T_2(80\text{ K})/T_2 > 1$ (above 60 K the Redfield corrected $1/T_2$ is nearly temperature independent), one can observe that in both samples T^* decreases upon proton irradiation. The T^* defined here has nothing to do with the pseudogap opening temperature in cuprates.

In the pristine sample ($x = 0.068$) $T^* \sim T_c = 23$ K while for the irradiated one ($\phi = 3.2 \times 10^{16}$ cm^{-2}) $T^* \sim 22$ K. In the overdoped compound ($x = 0.107$) the effect of irradiation on T^* is much bigger: In the irradiated (3.2×10^{16} cm^{-2}) sample $T^* = 12.5$ K while the pristine sample value is $T^* = 18$ K. Hence in the overdoped compounds the T^* shift upon irradiation ($\Delta T^* \sim 6$ K) is much bigger than the T_c shift ($\Delta T_c \sim 1$ K).

III. DISCUSSION

Let us first consider the rich phenomenology displayed by the ^{75}As NMR line width (Figs. 4 and 5). In the optimally doped sample ($x = 0.068$) $\Delta\nu$ increases at low temperature for all the dose levels (see Fig. 4). Conversely, $\Delta\nu$ is flat at high temperature ($T > 60$ K) and its value is only weakly dependent on the total proton fluence. In the former compound it is possible to fit the line width temperature dependence with a Curie Weiss law:

$$\Delta\nu = \Delta\nu_0 + \frac{C}{T+\theta}, \tag{5}$$

where $\Delta\nu_0$ is a temperature independent component, C is the Curie constant, and θ the Curie-Weiss temperature. The fit parameters are summarized in Table II. The Curie Weiss behavior of the linewidth and the observation that for $T < 50$ K $\Delta\nu$ decreases upon decreasing the magnetic field intensity indicate that the low temperature broadening is associated with the modulation of the local magnetic field at the nuclei induced by the electron spin texture.

TABLE II. Curie constant C and Curie-Weiss temperature θ obtained from the analysis of the temperature evolution of the ^{75}As NMR central line width $\Delta\nu$ shown in Fig. 4 for $Ba(Fe_{0.932}Rh_{0.068})_2As_2$. The temperature independent term $\Delta\nu_0$ is equal to 21.5 kHz.

ϕ (cm^{-2})	C (kHz K)	θ (K)
0	420 ± 40	20 ± 4
3.2×10^{16}	460 ± 50	5 ± 3
6.4×10^{16}	440 ± 40	-6.5 ± 1.5

The high temperature line width, $\Delta\nu_0 \simeq 21.5$ kHz, is due to the sum of nuclear dipolar line broadening, of the quadrupolar broadening and possibly of the magnetic broadening [$\Delta\nu_{\text{magnetic}} \propto M(T,H_0) \propto \chi(T)H_0$]. From dipolar sums it can be found that the nuclear dipolar contribution is actually very small (<2 kHz) [38,49]. The quadrupolar broadening should be zero for $H \parallel c$, however the misalignment by an angle ϑ may lead to some broadening of the central ^{75}As NMR line, which can be estimated from [50]

$$\Delta\nu_{0_Q} \sim \frac{3\nu_Q \Delta\nu_Q}{\nu_L}\vartheta^2 , \tag{6}$$

where ν_Q is the splitting between the central line ($\frac{1}{2} \rightarrow -\frac{1}{2}$) and the satellite line ($\frac{1}{2} \rightarrow \frac{3}{2}$), $\Delta\nu_Q$ the width of the satellite, $\nu_L = \gamma H_0/2\pi$ the Larmor frequency. In the $x = 0.068$ sample $\nu_Q \sim 2.3$ MHz and $\Delta\nu_Q \sim 1$ MHz. The value of ν_Q depends on the electric quadrupole interaction between the quadrupole moment of the ^{75}As nuclei and the electric field gradient (EFG) generated by the electron density. The width of the satellite lines is mainly due to the EFG inhomogeneity originating from Rh doping. The spectrum of the $Ba(Fe_{0.932}Rh_{0.068})_2As_2$ high frequency satellite line is reported in Fig. 9, the signal

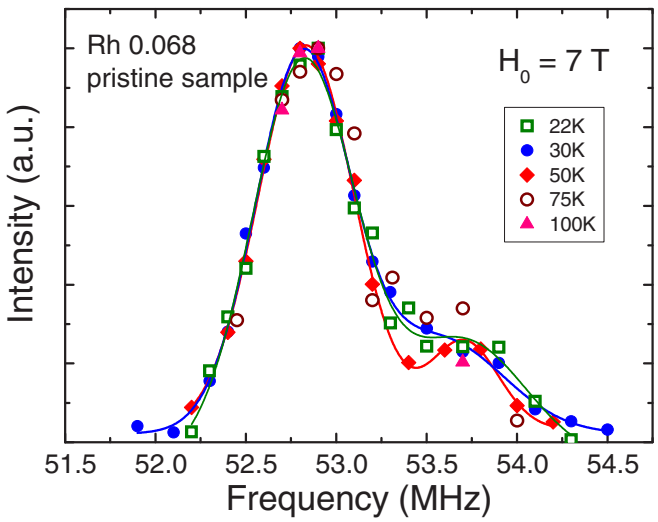

FIG. 9. Spectra of the high frequency satellite line of $Ba(Fe_{0.932}Rh_{0.068})_2As_2$ for various temperatures. The intensity is the integral of the spin echo and the solid lines are fits to a double Gaussian. The amplitude of the low frequency peak is three times that of the high frequency peak. The high frequency peak is thus the signal from ^{75}As nuclei near neighbors of Rh in the $x = 0.068$ sample, which are roughly 1/4 of the total [52].

from the ^{75}As near neighbors of Rh can clearly be seen in the spectrum. If one considers that the misalignment $\vartheta < 10^\circ$ one finds that the quadrupolar broadening $\Delta\nu_{0_Q} \leqslant 10$ kHz, still much smaller than $\Delta\nu_0$. It is then likely that the temperature independent magnetic broadening has to be associated with the T-independent component of the electron spin susceptibility, similarly to that reported by Mukhopadhyay *et al.* [49] in $Ba_{1-x}K_xFe_2As_2$.

The Curie-Weiss $\Delta\nu$ behavior indicates the presence of spin correlations and was often observed in the cuprates in the presence of defects [51]. In fact, the impurities induce a local spin polarization $\langle S_z\rangle$ on the conduction electrons which leads to a spatially varying spin polarization $s(\mathbf{r}) = \chi(\mathbf{r})\langle S_z\rangle$. The resulting NMR spectrum is the histogram of the spin polarization probed by the nuclei and the line width at a given temperature depends on the temperature evolution of $\chi(\mathbf{r})$. Accordingly, $\Delta\nu$ follows the susceptibility of the local moments which can be described by a Curie-Weiss law [51].

The small low temperature line broadening already present in the pristine $x = 0.068$ sample is likely due to the presence of defects related to Rh doping. For this composition in fact the spin correlation are still strong and thus some line broadening due to intrinsic defects is not unexpected. This line width increase is probably unrelated to the presence of Fe vacancies since the stoichiometry of the grown crystals was observed to be very close to the nominal one.

Remarkably, for $\phi = 6.4 \times 10^{16}$ cm^{-2}, the Curie-Weiss temperature becomes negative, signaling the shift of the correlations from antiferromagnetic to ferromagnetic. Ferromagnetic correlations were detected in other compounds of the 122 family, in particular in the nonsuperconducting $Ba(Fe_{1-x}Mn_x)_2As_2$ [53] and, with a much lower θ, in the superconducting $Ba(Fe_{1-x}Co_x)_2As_2$ and $BaFe_2(As_{1-x}P_x)_2$ [54] after the introduction of Mn impurities. Ferromagnetic fluctuations were also observed in hole and electron doped $BaFe_2As_2$ [55] and in $Ca(Fe_{1-x}Co_x)_2As_2$ [56]. The observed $\Delta\nu$ temperature dependence is analogous to the one measured in Mn-doped $LaFe_{1-y}Mn_yAsO_{1-x}F_x$, where the introduction of tiny amounts of Mn strongly suppresses T_c and gives rise to a significant increase of ^{19}F NMR line width [57,58]. However, in $LaFe_{1-y}Mn_yAsO_{1-x}F_x$, θ is always positive and the introduction of magnetic impurities enhances both θ and C, indicating that Mn doping strengthens the spin correlations already present in the Mn free compound. On the other hand, in proton irradiated $Ba(Fe_{0.932}Rh_{0.068})_2As_2$, the value of C remains unchanged and θ first decreases and then changes sign upon increasing the dose.

It should be noticed that, at variance with Mn doping, the lattice defects created by proton irradiation are nonmagnetic. Even though the rise of magnetism upon ion irradiation was observed in several materials [59], we recall that the Ba122 family of iron-based superconductors is quite unstable towards impurity driven static magnetism [49,60]. Hence, the observation that the nonmagnetic defects introduced by irradiation lead to enhanced spin correlations and to a broadening of the NMR lines is not unexpected. Indeed, it is well known that by doping $YBaCu_3O_{6+x}$ with nonmagnetic Zn and Li [51] impurities the ^{89}Y NMR line gets structured [61] and its line width follows a Curie law [51,62]. Since Zn impurities are expected to behave like Cu vacancies in $YBaCu_3O_{6+x}$ [51]

one could conclude that Fe and Cu vacancies indeed have a similar behavior. However the case of proton induced damage is not identical to that of Fe vacancies since the defects induced by radiation affects all the crystal sites.

In the overdoped compound the behavior of the linewidth is utterly different from that of the optimally doped (see Fig. 5). The pristine sample displays a completely flat $\Delta\nu(T)$ down to 9 K and then a rapid increase, likely due to the freezing of the vortex motions [63]. In the irradiated sample ($\phi = 6.4 \times 10^{16}$ cm^{-2}) $\Delta\nu$ reaches a maximum around 18 K and then decreases slightly at lower temperatures. Interestingly the temperature at which the line width of the irradiated sample starts to decrease is close to the temperature T^* at which the spin-spin relaxation rate begins to rise and the echo decay becomes a single exponential. This suggests that the low frequency spin fluctuations, which are responsible for the $1/T_2$ enhancement, partially average out the static frequency distribution probed by the ^{75}As nuclei.

We will now discuss the effect of irradiation on $1/T_2$. The marked increase of $1/T_2$ starting at $T^* > T_c$ seems to be a common feature of several 122 compounds [38,39,63]. In Ref. [39] we showed that this effect is unrelated to the superconducting state and that T^* can become much higher than T_c in the presence of a high magnetic field. As we already explained in the previous section the $1/T_2$ enhancement below T^* is affected by proton irradiation. The increase in $1/T_2$ was associated with slow nematic fluctuations between $(\pi,0)$ and $(0,\pi)$ ground states, very much akin to the nematic fluctuations found in prototypes of the J_1-J_2 model on a square lattice [64,65]. These low-frequency fluctuations have been predicted [66] in the iron based superconductors and nematic fluctuations have subsequently been observed in several underdoped [67–69] and overdoped IBS [38,39].

In the presence of these fluctuations $1/T_2$ can be written as [39,70]:

$$\frac{1}{T_2} = a(\Delta\nu(T))^2\tau_D(T) + \frac{1}{T_{2_i}} \tag{7}$$

with τ_D the characteristic fluctuation time, a a dimensionless coupling constant, and T_{2_i} the T-independent contribution to the relaxation arising from nuclear dipole-dipole interaction. The resulting temperature dependent $\tau_D(T)$ can then be fitted to an Arrhenius law $\tau_D(T) = \tau_0 e^{U/T}$ where U is the activation energy and τ_0, the high temperature characteristic time of the fluctuations, in the nanosecond range. We fitted the $1/T_2$ data using Eq. (7) in the 20–26 K temperature range for $x = 0.068$ and in the 7–30 K range for $x = 0.107$.

In the pristine samples we found that, for $x = 0.068$, the activation energy is $U \simeq 200 \pm 30$ K while in the overdoped $x = 0.107$ sample $U \simeq 40 \pm 20$ K, in good agreement with the values obtained in Refs. [38,39]. Upon proton irradiation U increases markedly in the optimally doped sample ($U \sim 500 \pm 100$ K for $\phi = 3.2 \times 10^{16}$ cm^{-2}) while it remains basically unchanged in the overdoped sample. Unfortunately, the quality of the fit decreases with increasing dose, pointing out that possibly the dynamics can no longer be described by a single activation barrier and that a distribution of energy barriers should be considered. This fact is particularly evident in the overdoped sample where the increase of $1/T_2$ becomes significantly sharper and T^* decrease by ∼6 K (Fig. 6). The substantial enhancement of the activation energy suggests that the presence of the defects slows down the fluctuations between the $(0,\pi)$ and $(\pi,0)$ ground states. It is remarked that such an effect has also been detected in the prototypes of the J_1-J_2 model on a square lattice doped with nonmagnetic impurities [71].

IV. CONCLUSIONS

In conclusion, we have shown that proton irradiation (5.5 MeV) in $Ba(Fe_{1-x}Rh_x)_2As_2$ results in a very weak T_c suppression, in good agreement with previous experiments carried out in other 122 compounds [13,14]. By measuring the ^{75}As NMR spectra we have evidenced that the defects introduced by proton irradiation induce ferromagnetic correlations in the optimally electron doped $x = 0.068$ compound. Remarkably this effect is totally absent in the overdoped sample owing to the absence of significant spin correlations. Moreover the analysis of the spin echo decay rate $(1/T_2)$ shows that the low-frequency fluctuations observed [34,35,67–69] in several families of iron based superconductors are damped by the irradiation induced impurities, consistently with the hypothesis that they could be associated with the presence of nematic fluctuations between $(0,\pi)$ and $(\pi,0)$ nematic phases.

ACKNOWLEDGMENTS

This work was supported by MIUR-PRIN2012 Project No. 2012X3YFZ2 and MIUR-PRIN2015 Project No. 2015C5SEJJ. The irradiations were performed in the framework of the INFN-Politecnico di Torino M.E.S.H. Research Agreement. The work at the Ames Laboratory was supported by the DOE-Basic Energy Sciences under Contract No. DE-AC02-07CH11358. The authors wish to thank the INFN-LNL staff for their support in the irradiation experiments.

[1] F. Massee, P. Oliver Sprau, Y.-L. Wang, J. C. S. Davis, G. Ghigo, G. Gu, and W.-K. Kwok, Science Advances **1**, e1500033 (2015).

[2] T. Tamegai, T. Taen, H. Yagyuda, Y. Tsuchiya, S. Mohan, T. Taniguchi, Y. Nakajima, S. Okayasu, M. Sasase, H. Kitamura, T. Murakami, T. Kambara, and Y. Kanai, Supercond. Sci. Technol. **25**, 084008 (2012).

[3] G. P. Summers, E. A. Burke, D. B. Chrisey, M. Nastasi, and J. R. Tesmer, Appl. Phys. Lett. **55**, 1469 (1989).

[4] F. Rullier-Albenque, P. A. Vieillefond, H. Alloul, A. W. Tyler, P. Lejay, and J. F. Marucco, Europhys. Lett. **50**, 81 (2000).

[5] R. J. Radtke, K. Levin, H.-B. Schüttler, and M. R. Norman, Phys. Rev. B **48**, 653(R) (1993).

[6] R. Prozorov, M. A. Tanatar, B. Roy, N. Ni, S. L. Bud'ko, P. C. Canfield, J. Hua, U. Welp, and W. K. Kwok, Phys. Rev. B **81**, 094509 (2010).

[7] N. W. Salovich, Hyunsoo Kim, A. K. Ghosh, R. W. Giannetta, W. Kwok, U. Welp, B. Shen, S. Zhu, H.-H. Wen, M. A. Tanatar, and R. Prozorov, Phys. Rev. B **87**, 180502(R) (2013).

[8] F. Laviano, R. Gerbaldo, G. Ghigo, L. Gozzelino, G. P. Mikitik, T. Taen, and T. Tamegai, Supercond. Sci. Technol. **27**, 044014 (2014).

[9] N. Haberkorn, J. Kim, B. Maiorov, I. Usov, G. F. Chen, W. Yu, and L. Civale, Supercond. Sci. Technol. **27**, 095004 (2014).

[10] F. Ohtake, T. Taen, S. Pyon, T. Tamegai, and S. Okayasu, Physics Procedia **58**, 122 (2014).

[11] K. J. Kihlstrom, L. Fang, Y. Jia, B. Shen, A. E. Koshelev, U. Welp, G. W. Crabtree, W.-K. Kwok, A. Kayani, S. F. Zhu, and H.-H. Wen, Appl. Phys. Lett. **103**, 202601 (2013).

[12] T. Taen, H. Yagyuda, Y. Nakajima, T. Tamegai, S. Okayasu, H. Kitamura, T. Murakami, F. Laviano, and G. Ghigo, Physica C **484**, 62 (2013).

[13] Y. Nakajima, T. Taen, Y. Tsuchiya, T. Tamegai, H. Kitamura, and T. Murakami, Phys. Rev. B **82**, 220504(R) (2010).

[14] T. Taen, F. Ohtake, H. Akiyama, H. Inoue, Y. Sun, S. Pyon, T. Tamegai, and H. Kitamura, Phys. Rev. B **88**, 224514 (2013).

[15] N. Haberkorn, B. Maiorov, I. O. Usov, M. Weigand, W. Hirata, S. Miyasaka, S. Tajima, N. Chikumoto, K. Tanabe, and L. Civale, Phys. Rev. B **85**, 014522 (2012).

[16] Y. Mizukami, M. Konczykowski, Y. Kawamoto, S. Kurata, S. Kasahara, K. Hashimoto, V. Mishra, A. Kreisel, Y. Wang, P. J. Hirschfeld, Y. Matsuda, and T. Shibauchi, Nat. Commun. **5**, 5657 (2014).

[17] R. Prozorov, M. Konczykowski, M. A. Tanatar, A. Thaler, S. L. Bud'ko, P. C. Canfield, V. Mishra, and P. J. Hirschfeld, Phys. Rev. X **4**, 041032 (2014).

[18] C. J. van der Beek, S. Demirdis, D. Colson, F. Rullier-Albenque, Y. Fasano, T. Shibauchi, Y. Matsuda, S. Kasahara, P. Gierlowski, and M. Konczykowski, J. Phys. Conf. Ser. **449**, 012023 (2013).

[19] K. Cho, M. Konczykowski, J. Murphy, H. Kim, M. A. Tanatar, W. E. Straszheim, B. Shen, H. H. Wen, and R. Prozorov, Phys. Rev. B **90**, 104514 (2014).

[20] K. Cho, M. K. Teknowijoyo, M. A. Tanatar, Yong Liu, T. A. Lograsso, W. E. Straszheim, V. Mishra, S. Maiti, P. J. Hirschfeld, and R. Prozorov, Science Advances **2**, e1600807 (2016).

[21] S. Teknowijoyo, K. Cho, M. A. Tanatar, J. Gonzales, A. E. Böhmer, O. Cavani, V. Mishra, P. J. Hirschfeld, S. L. Bud'ko, P. C. Canfield, and R. Prozorov, Phys. Rev. B **94**, 064521 (2016).

[22] I. I. Mazin, D. J. Singh, M. D. Johannes, and M. H. Du, Phys. Rev. Lett. **101**, 057003 (2008).

[23] A. V. Chubukov, D. V. Efremov, and I. Eremin, Phys. Rev. B **78**, 134512 (2008).

[24] R. M. Fernandes, M. G. Vavilov, and A. V. Chubukov, Phys. Rev. B **85**, 140512(R) (2012).

[25] Yunkyu Bang and G. R. Stewart, J. Phys.: Condens. Matter **29**, 123003 (2017).

[26] G. Ghigo, G. A. Ummarino, L. Gozzelino, R. Gerbaldo, F. Laviano, D. Torsello, and T. Tamegai (unpublished).

[27] J. Li, Y. Guo, S. Zhang, Y. Tsujimoto, X. Wang, C. I. Sathish, S. Yu, K. Yamaura, and E. Takayama-Muromachi, Solid State Commun. **152**, 671 (2012).

[28] Y. Li, X. Lin, Q. Tao, C. Wang, T. Zhou, L. Li, Q. Wang, M. He, G. Cao, and Z. Xu, New J. Phys. **11**, 053008 (2009).

[29] Y. Li, J. Tong, Q. Tao, C. Feng, G. Cao, W. Chen, F.-c. Zhang, and Z.-a. Xu, New J. Phys. **12**, 083008 (2010).

[30] Y. F. Guo, Y. G. Shi, S. Yu, A. A. Belik, Y. Matsushita, M. Tanaka, Y. Katsuya, K. Kobayashi, I. Nowik, I. Felner, V. P. S. Awana, K. Yamaura, and E. Takayama-Muromachi, Phys. Rev. B **82**, 054506 (2010).

[31] H. Kim, M. A. Tanatar, W. E. Straszheim, K. Cho, J. Murphy, N. Spyrison, J.-Ph. Reid, Bing Shen, H.-H. Wen, R. M. Fernandes, and R. Prozorov, Phys. Rev. B **90**, 014517 (2014).

[32] J.-Ph. Reid, M. A. Tanatar, X. G. Luo, H. Shakeripour, S. R. de Cotret, A. Juneau-Fecteau, J. Chang, B. Shen, H.-H. Wen, H. Kim, R. Prozorov, N. Doiron-Leyraud, and L. Taillefer, Phys. Rev. B **93**, 214519 (2016).

[33] A. V. Chubukov, M. Khodas, and R. M. Fernandes, Phys. Rev. X **6**, 041045 (2016).

[34] N. J. Curro, A. P. Dioguardi, N. ApRoberts-Warren, A. C. Shockley, and P. Klavins, New J. Phys. **11**, 075004 (2009).

[35] H. Xiao, T. Hu, A. P. Dioguardi, N. apRoberts-Warren, A. C. Shockley, J. Crocker, D. M. Nisson, Z. Viskadourakis, X. Tee, I. Radulov, C. C. Almasan, N. J. Curro, and C. Panagopoulos, Phys. Rev. B **85**, 024530 (2012).

[36] A. P. Dioguardi, M. M. Lawson, B. T. Bush, J. Crocker, K. R. Shirer, D. M. Nisson, T. Kissikov, S. Ran, S. L. Bud'ko, P. C. Canfield, S. Yuan, P. L. Kuhns, A. P. Reyes, H.-J. Grafe, and N. J. Curro, Phys. Rev. B **92**, 165116 (2015).

[37] T. Kissikov, A. P. Dioguardi, E. I. Timmons, M. A. Tanatar, R. Prozorov, S. L. Bud'ko, P. C. Canfield, R. M. Fernandes, and N. J. Curro, Phys. Rev. B **94**, 165123 (2016).

[38] L. Bossoni, P. Carretta, W. P. Halperin, S. Oh, A. Reyes, P. Kuhns, and P. C. Canfield, Phys. Rev. B **88**, 100503(R) (2013).

[39] L. Bossoni, M. Moroni, M. H. Julien, H. Mayaffre, P. C. Canfield, A. Reyes, W. P. Halperin, and P. Carretta, Phys. Rev. B **93**, 224517 (2016).

[40] N. Ni, M. E. Tillman, J.-Q. Yan, A. Kracher, S. T. Hannahs, S. L. Bud'ko, and P. C. Canfield, Phys. Rev. B **78**, 214515 (2008); N. Ni, A. Thaler, A. Kracher, J.-Q. Yan, S. L. Bud'ko, and P. C. Canfield, *ibid.* **80**, 024511 (2009).

[41] M. A. Tanatar, N. Ni, C. Martin, R. T. Gordon, H. Kim, V. G. Kogan, G. D. Samolyuk, S. L. Bud'ko, P. C. Canfield, and R. Prozorov, Phys. Rev. B **79**, 094507 (2009).

[42] M. A. Tanatar, N. Ni, S. L. Bud'ko, P. C. Canfield, and R. Prozorov, Supercond. Sci. Technol. **23**, 054002 (2010).

[43] M. A. Tanatar, R. Prozorov, N. Ni, S. L. Bud'ko, and P. C. Canfield, U. S. Patent 8, 450, 246.

[44] M. A. Tanatar, N. Ni, A. Thaler, S. L. Bud'ko, P. C. Canfield, and R. Prozorov, Phys. Rev. B **82**, 134528 (2010).

[45] J. F. Ziegler, http://www.srim.org/

[46] R. E. Stoller, M. B. Toloczko, G. S. Was, A. G. Certain, S. Dwaraknath, and F. A. Gardner, Nucl. Instrum. Meth. B **310**, 75 (2013).

[47] A. G. Redfield and W. N. Yu, Phys. Rev. **169**, 443 (1968).

[48] R. E. Walstedt and S.-W. Cheong, Phys. Rev. B **51**, 3163 (1995).

[49] S. Mukhopadhyay, S. Oh, A. M. Mounce, M. Lee, W. P. Halperin, N. Ni, S. L. Bud'ko, P. C. Canfield, A. P. Reyes, and P. L. Kuhns, New J. Phys. **11**, 055002 (2009).

[50] A. Abragam, *Principles of Nuclear Magnetism* (Oxford University Press, New York, 1961).

[51] H. Alloul, J. Bobroff, M. Gabay, and P. J. Hirschfeld, Rev. Mod. Phys. **81**, 45 (2009).

[52] M. Mazzani, P. Bonfà, G. Allodi, S. Sanna, A. Martinelli, A. Palenzona, P. Manfrinetti, M. Putti, and R. De Renzi, Phys. Status Solidi B **251**, 974 (2014).
[53] D. LeBoeuf, Y. Texier, M. Boselli, A. Forget, D. Colson, and J. Bobroff, Phys. Rev. B **89**, 035114 (2014).
[54] Y. Texier, Y. Laplace, P. Mendels, J. T. Park, G. Friemel, D. L. Sun, D. S. Inosov, C. T. Lin, and J. Bobroff, Europhys. Lett. **99**, 17002 (2012).
[55] P. Wiecki, B. Roy, D. C. Johnston, S. L. Bud'ko, P. C. Canfield, and Y. Furukawa, Phys. Rev. Lett. **115**, 137001 (2015).
[56] J. Cui, P. Wiecki, S. Ran, S. L. Bud'ko, P. C. Canfield, and Y. Furukawa, Phys. Rev. B **94**, 174512 (2016).
[57] F. Hammerath, M. Moroni, L. Bossoni, S. Sanna, R. Kappenberger, S. Wurmehl, A. U. B. Wolter, M. A. Afrassa, Y. Kobayashi, M. Sato, B. Büchner, and P. Carretta, Phys. Rev. B **92**, 020505(R) (2015).
[58] M. Moroni, S. Sanna, G. Lamura, T. Shiroka, R. De Renzi, R. Kappenberger, M. A. Afrassa, S. Wurmehl, A. U. B. Wolter, B. Büchner, and P. Carretta, Phys. Rev. B **94**, 054508 (2016).
[59] P. Esquinazi, W. Hergert, D. Spemann, A. Setzer, and A. Ernst, Transaction on Magnetics **49**, 4668 (2013).
[60] T. Goko, A. A. Aczel, E. Baggio-Saitovitch, S. L. Bud'ko, P. C. Canfield, J. P. Carlo, G. F. Chen, P. Dai, A. C. Hamann, W. Z. Hu, H. Kageyama, G. M. Luke, J. L. Luo, B. Nachumi, N. Ni, D. Reznik, D. R. Sanchez-Candela, A. T. Savici, K. J. Sikes, N. L. Wang, C. R. Wiebe, T. J. Williams, T. Yamamoto, W. Yu, and Y. J. Uemura, Phys. Rev. B **80**, 024508 (2009).
[61] H. Alloul, P. Mendels, H. Casalta, J. F. Marucco, and J. Arabski, Phys. Rev. Lett. **67**, 3140 (1991).
[62] A. V. Mahajan, H. Alloul, G. Collin, and J. F. Marucco, Phys. Rev. Lett. **72**, 3100 (1994).
[63] S. Oh, A. M. Mounce, S. Mukhopadhyay, W. P. Halperin, A. B. Vorontsov, S. L. Bud'ko, P. C. Canfield, Y. Furukawa, A. P. Reyes, and P. L. Kuhns, Phys. Rev. B **83**, 214501 (2011).
[64] P. Carretta, R. Melzi, N. Papinutto, and P. Millet, Phys. Rev. Lett. **88**, 047601 (2002).
[65] P. Chandra, P. Coleman, and A. I. Larkin, Phys. Rev. Lett. **64**, 88 (1990).
[66] I. I. Mazin and M. D. Johannes, Nat. Phys. **5**, 141 (2009).
[67] M. Fu, D. A. Torchetti, T. Imai, F. L. Ning, J.-Q. Yan, and A. S. Sefat, Phys. Rev. Lett. **109**, 247001 (2012).
[68] T. Iye, M.-H. Julien, H. Mayaffre, M. Horvatić, C. Berthier, K. Ishida, H. Ikeda, S. Kasahara, T. Shibauchi, and Y. Matsuda, J. Phys. Soc. Jpn. **84**, 043705 (2015).
[69] R. Zhou, L. Y. Xing, X. C. Wang, C. Q. Jin, and Guo-qing Zheng, Phys. Rev. B **93**, 060502 (2016).
[70] C. P. Slichter, *Principles of Magnetic Resonance*, Cap. 5.12, Third Enlarged and Updated Edition, Springer Series In Solid-State Sciences (Springer-Verlag, Berlin Heidelberg, 1996).
[71] N. Papinutto, P. Carretta, S. Gonthier, and P. Millet, Phys. Rev. B **71**, 174425 (2005).